IEEE Access
Multidisciplinary | Rapid Review | Open Access Journal

Received July 24, 2019, accepted August 14, 2019, date of publication August 20, 2019, date of current version September 4, 2019.

Digital Object Identifier 10.1109/ACCESS.2019.2936420

Single-Phase-to-Earth Faulty Feeder Detection in Power Distribution Network Based on Amplitude Ratio of Zero-Mode Transients

NAN PENG[1], (Student Member, IEEE), KAI YE[1], RUI LIANG[1], (Member, IEEE), TIANYU HOU[1], GUANHUA WANG[1], XUAN CHEN[2], AND SONG TENG[3]

[1]School of Electrical and Power Engineering, China University of Mining and Technology, Xuzhou 221116, China
[2]State Grid Jiangsu Electric Power Company Maintenance Branch, Nanjing 210000, China
[3]State Grid Xuzhou Power Supply Company, Xuzhou 221005, China

Corresponding author: Rui Liang (liangrui@ cumt.edu.cn)

This work was supported in part by the Natural Science Foundation of Jiangsu Province under Grant BK20161185, in part by the "Six Talents Summit" High-level Talents Project of Jiangsu Province under Grant XNY-046, in part by the Science and Technology Program of State Grid Jiangsu Electric Power Company Ltd., under Grant J2018036, and in part by the Science and Technology Program of State Grid under Grant J2018078.

ABSTRACT The single-phase-to-earth fault (SPTEF) current is weak in neutral ineffectively grounded systems. High fault impedance, noise and arc impair the fault feature, which increases the difficulty of faulty feeder detection. Based on the propagation characteristics of zero-mode transients (ZTs), this paper proposes a faulty feeder detection criterion by utilizing the amplitude information of the ZTs captured at both terminals. To conduct the criterion, the historical data of the ZTs recorded at both terminals of each feeder with a bus fault is collected. The standard amplitude ratios of the frequency components in the ZTs of each feeder are extracted by S-transform. After a SPTEF is detected in the system, the actual amplitude ratios of the ZTs are calculated and compared with the standard ones. Theoretical analysis and simulation indicate that the maximum ratio between the standard and actual ratios corresponds to the faulty feeder. In implementation of the criterion, both high sampling frequency and accurate synchronization are not required. A 10kV single-end radial distribution network is constructed by PSCAD/EMTDC. Various fault simulations are carried out and the calculation results demonstrate that the proposed criterion has high reliability and is not affected by neutral grounding mode, fault initial condition, high impedance fault (HIF) and noise.

INDEX TERMS Zero-mode transients, amplitude ratio, faulty feeder detection, distribution network.

I. INTRODUCTION

Fast and reliable fault detection has become a fundamental requirement of modern distribution network [1]. Due to the weak SPTEF currents in non-effectively grounded distribution system, it is difficult to detect the faulty feeder with complex factors (HIFs and noises). Thus, faulty feeder detection has become a hot research topic in power system protection. Many scholars at home and abroad have made substantial and useful explorations on faulty feeder detection.

The associate editor coordinating the review of this article and approving it for publication was Amedeo Andreotti.

According to the source of the detected signal, faulty feeder detection methods can be divided into two main categories: active methods [2]–[4] and passive methods. The active methods need additional equipment, which restricts the application of these methods. Different from the active methods, the real-time measurements are utilized in the passive methods to achieve online faulty feeder detection, which leads to the promising applications of these methods. Based on the signal characteristics, the passive methods are further classified into two types: steady-state [5], [6] and transient methods [7]–[11]. The steady-state ones mainly utilize the difference of the amplitudes (or phases) of the steady-state currents, the polarities of the active or harmonic components [12],

and zero-sequence admittances [13] between the faulty and sound feeders. The steady-state methods have clear physical meaning, which makes them easy to be applied in actual field. However, they may be susceptible to the fault conditions, such as feeder parameters, fault resistances, neutral grounding modes, etc. [14].

When a SPTEF occurs in a distribution feeder, the fault transient components, whose amplitudes can be as several or dozens times of those of the steady-state ones, contain abundant and useful fault information [10]. Based on the distribution characteristics of zero-sequence currents [15], relationship between zero-sequence voltages and currents [16], transient power directions, or energy of zero-sequence currents [17], the transient methods can identify the faulty feeder with different neutral grounding modes including the solidly and resister ones. In general, the transient methods have high reliability, great sensitivity [18], and fast response in complex fault conditions. Reference [19] firstly extracts the wavelet modulus maximum to obtain the arrival time of initial transient traveling waves. Then, the faulty feeder is detected by comparing the amplitudes and polarities of zero-mode currents. In reference [20], the faulty feeder is identified by using the wavelet modulus maxima of initial transient current and voltage traveling waves. In addition, some new types of the intelligent algorithms [21], [22], commonly utilized to extract the signal features, have been integrated into faulty feeder detection and show promising results.

Although many faulty feeder detection methods have been proposed, some of them may require additional equipment [2]–[4], some of them do not consider the arc faults [5], [7], [10], [13], [19], some of them [6]–[11], [15]–[20] are susceptible to strong noise interference, and some others [21], [22] need substantial training samples. Besides, the method in [14] may be affected by system parameters, the methods in [7], [9], [10], [13] need to set thresholds to detect the faulty feeder, and the methods in [12] and [17] may be affected by the values of harmonic and active components.

In order to address the above problems, this paper firstly utilizes the fault-generated transients which can be reliably detected in both ordinary and high-impedance faults. Second, mathematical morphology combined with S-transform is adopted to process the noised ZTs, which shows promising anti-noise ability. Third, only one set of historical data of the ZTs, easy to be obtained in a bus fault, is needed to conduct the faulty feeder detection. Last, different from the current traveling wave methods, the accurate arrival time and wave velocity are not needed. The main contributions of this paper are as follows:

- Based on the propagation characteristics of the ZTs, the mathematical expression of the amplitude ratio of the ZTs measured at both terminals of each feeder is derived for both bus and feeder faults.
- A faulty feeder detection criterion based on the maximum ratio of the standard and actual amplitude ratios of the ZTs is constructed.

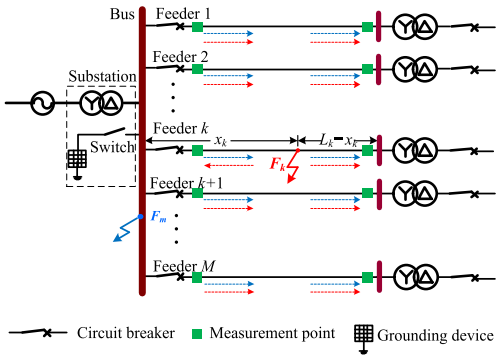

FIGURE 1. Diagram of a single-terminal radial distribution network.

- The criterion is not affected by complex fault conditions and strong noises. In addition, accurate synchronization and high sampling frequency are not required.

II. MATHEMATICAL REPRESENTATIONS OF THE AMPLITUDE RATIOS OF ZTS

After a SPTEF occurs in a distribution feeder, the wave front signal $S^{(0)}(x)$ of the ZT which propagates x from the fault point can be expressed by [23]

$$\begin{cases} S^{(0)}(x) = \sum\limits_i e^{-\gamma_i^{(0)} x} \cdot S_i^{(0)} = \sum\limits_i e^{-\left(\alpha_i^{(0)} + j\cdot\beta_i^{(0)}\right)x} \cdot \frac{A}{\omega_i} \\ \gamma_i^{(0)} = \sqrt{Z_i^{(0)} \cdot Y_i^{(0)}} = \alpha_i^{(0)} + j\beta_i^{(0)} \end{cases} \tag{1}$$

where $S_i^{(0)}$ represents the initial amplitude of the component with angular frequency ω_i in the wave front signal. A is the amplitude of the initial ZT at the fault point. $\gamma_i^{(0)}$ is the zero-mode propagation constant whose real part $\alpha_i^{(0)}$ and imaginary part $\beta_i^{(0)}$ are the amplitude attenuation and phase lag coefficients with ω_i. $Z_i^{(0)}$ and $Y_i^{(0)}$ denote the zero-mode impedance and admittance in per unit length of the feeder. Rearranging (1), we have

$$S^{(0)}(x) = \sum_i S_{amp}^{(0)} \cdot S_{pha}^{(0)} = \sum_i \left(e^{-\alpha_i^{(0)} x} \frac{A}{\omega_i} \right) \cdot e^{-j\beta_i^{(0)} x} \tag{2}$$

In (2), $S_{amp}^{(0)}$ and $S_{pha}^{(0)}$ are the amplitude and phase of $S^{(0)}(x)$ with ω_i. According to (2), it can be observed that $S^{(0)}(x)$ is composed of a large variety of frequency components whose amplitudes are in exponential attenuation with the increase of propagation distance. In general, the longer the propagation distance, the higher the frequency, and the more significant the amplitude attenuation [24].

A single-terminal radial distribution network is depicted in Fig.1 where the state of the switch in the substation determines the neutral grounding mode (ungrounded or arc-suppression coil (ASC) grounded) of the system. ASCs are widely adopted to reduce the steady-state fault current by compensating the steady-state capacitive grounding currents of healthy feeders. As for high-frequency transient currents, ASCs show high impedance, which blocks the current flows. Thus, there is no inductive transient current at the fault point,

which indicates that ASCs cannot compensate the fault-generated transients. The ZTs, whose frequencies are far higher than power frequency, are not affected by ASCs.

It is assumed that the network consists of M feeders and the length of feeder $j(1 \le j \le M)$ is L_j. Based on the propagation characteristics of ZTs, the amplitude ratio of the ZTs captured at both terminals of any feeder is analyzed.

When the fault point F_m is at bus, the propagation paths of ZTs are shown by the blue dotted arrows. For feeder j, the amplitudes of the ZTs with ω_i measured at both terminals can be shown as

$$\begin{cases} \left|U^{(0)}_{jm\_st}\right| = \dfrac{A}{\omega_i} \\ \left|U^{(0)}_{jm\_ed}\right| = \left|\rho_{j\_ed}\right| \cdot e^{-\alpha_i^{(0)} L_j} \cdot \dfrac{A}{\omega_i} \end{cases} \tag{3}$$

where $|U^{(0)}_{jm\_st}|$ and $|U^{(0)}_{jm\_ed}|$ represent the amplitudes of ZTs at starting and ending terminals of feeder j. ρ_{j_ed} is the reflection coefficient at the ending terminal. The definition of reflection coefficient is shown in Appendix A. According to (3), the ratio AP_{jm} of the amplitudes of the ZTs at both terminals can be formulated as

$$AP_{jm} = \frac{\left|U^{(0)}_{jm\_st}\right|}{\left|U^{(0)}_{jm\_ed}\right|} = \frac{1}{\left|\rho_{j\_ed}\right|} \cdot e^{\alpha_i^{(0)} L_j} \tag{4}$$

When the fault point F_k is in feeder k, the propagation paths of ZTs are shown by the red dotted arrows. For the faulty feeder k, the amplitudes of the ZTs with ω_i measured at both terminals can be presented as

$$\begin{cases} \left|U^{(0)}_{kf\_st}\right| = \left|\rho_{k\_st}\right| \cdot e^{-\alpha_i^{(0)} x_k} \cdot \dfrac{A}{\omega_i} \\ \left|U^{(0)}_{kf\_ed}\right| = \left|\rho_{k\_ed}\right| \cdot e^{-\alpha_i^{(0)} (L_k - x_k)} \cdot \dfrac{A}{\omega_i} \end{cases} \tag{5}$$

where $|U^{(0)}_{kf\_st}|$ and $|U^{(0)}_{kf\_ed}|$ represent the amplitudes of ZTs at starting and ending terminals of the faulty feeder k. ρ_{k_st} and ρ_{k_ed} are the reflection coefficients at the starting and ending terminals of feeder k. The ratio AP_{kf} of the amplitudes of the ZTs at both terminals shown in (5) can be acquired by

$$AP_{kf} = \frac{\left|U^{(0)}_{kf\_st}\right|}{\left|U^{(0)}_{kf\_ed}\right|} = \frac{\left|\rho_{k\_st}\right|}{\left|\rho_{k\_ed}\right|} \cdot e^{\alpha_i^{(0)} (L_k - 2x_k)} \tag{6}$$

For the sound feeder j ($j \ne k$), the amplitudes of the ZTs with ω_i measured at both terminals can be as described as

$$\begin{cases} \left|U^{(0)}_{jf\_st}\right| = \left|1 + \rho_{j\_st}\right| \cdot e^{-\alpha_i^{(0)} x_k} \cdot \dfrac{A}{\omega_i} \\ \left|U^{(0)}_{jf\_ed}\right| = \left|1 + \rho_{j\_st}\right| \cdot \left|\rho_{j\_ed}\right| e^{-\alpha_i^{(0)} (L_j + x_k)} \cdot \dfrac{A}{\omega_i} \end{cases} \tag{7}$$

In (7), $|U^{(0)}_{jf\_st}|$ and $|U^{(0)}_{jf\_ed}|$ denote the amplitudes of ZTs at starting and ending terminals of the sound feeder j. ρ_{j_st} and ρ_{j_ed} are the reflection coefficients at the starting and ending terminals of feeder j. Similarly, the ratio AP_{jf} of the amplitudes at both terminals shown in (7) is given by

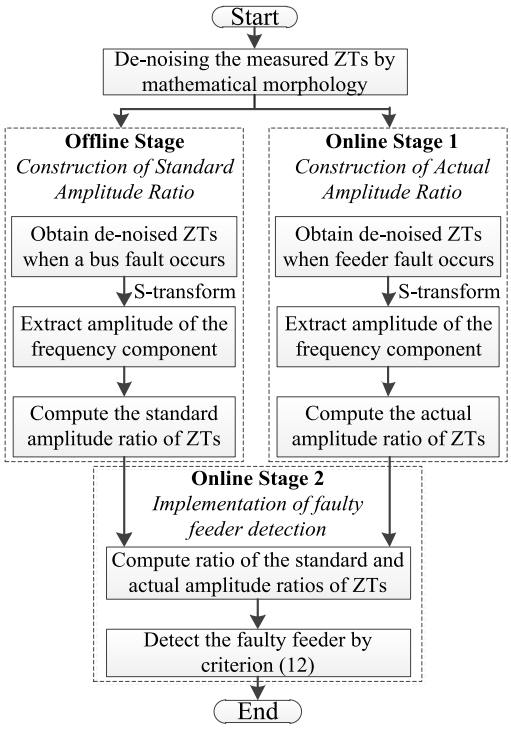

FIGURE 2. Flow chart of the faulty feeder detection.

$$AP_{jf} = \frac{\left|U^{(0)}_{jf\_st}\right|}{\left|U^{(0)}_{jf\_ed}\right|} = \frac{1}{\left|\rho_{j\_ed}\right|} \cdot e^{\alpha_i^{(0)} L_j} \tag{8}$$

It can be concluded from (4), (6) and (8) that the ratio of the ZTs captured at both terminals of each feeder is independent from the fault conditions (fault impedance and inception angles) whether the SPTEF occurs at bus or in the feeder.

III. FAULTY FEEDER DETECTION BASED ON THE AMPLITUDE RATIOS OF ZTS

In the two cases of bus and feeder k faults, as for feeder k, the ratio R_{jm-kf} of AP_{jm} (shown in (4)) to AP_{kf} (presented in (6)) can be derived as

$$R_{jm-kf} = \frac{\left|U^{(0)}_{jm\_st}\right|}{\left|U^{(0)}_{jm\_ed}\right|} \cdot \frac{\left|U^{(0)}_{kf\_ed}\right|}{\left|U^{(0)}_{kf\_st}\right|} = \frac{1}{\left|\rho_{k\_st}\right|} e^{\alpha_i^{(0)} 2x_k} \tag{9}$$

It is abundantly obvious that $R_{jm-kf} > 1$. Similarly, as for feeder j in the two cases mentioned above, the ratio R_{jm-jf} of AP_{jm} to AP_{jf} (in (8)) can be obtained by

$$R_{jm-jf} = \frac{\left|U^{(0)}_{jm\_st}\right|}{\left|U^{(0)}_{jm\_ed}\right|} \cdot \frac{\left|U^{(0)}_{jf\_ed}\right|}{\left|U^{(0)}_{jf\_st}\right|} = 1 \tag{10}$$

From (9) and (10), it is evident that

$$R_{jm-kf} > R_{jm-jf} \tag{11}$$

The relationship shown in (11) indicates that there exists a difference between R_{jm-kf} and R_{jm-jf} in the two fault cases, which can be utilized to construct the faulty feeder detection criterion. The flow chart of the faulty feeder detection criterion is displayed in Fig.2. Detailed stages are as follows.

♦ *Construction of standard amplitude ratio—— Offline stage*

First, the historical data of the ZTs is collected. To select the appropriate data, when the bus faults occur in a feeder of the distribution network, all the waveforms of ZT signals recorded by the measurement points at both terminals of each feeder should be collected and sorted for each bus fault event. Next, the bad data is eliminated, which can be realized by data cleansing algorithms. Then, to ensure calculation accuracy, the ZTs in the data set with the largest amplitudes are selected to construct the standard amplitude ratio. Finally, the amplitudes of the frequency components with ω_i in the selected ZTs are extracted by S-transform. The standard amplitude ratio for each feeder can be determined by computing the ratio between the frequency component amplitude at the starting terminal and that at the ending terminal.

♦ *Construction of actual amplitude ratio—— Online stage*1

First, the actual ZTs at both terminals of each feeder when a SPTEF is detected in a feeder is measured. Second, the amplitudes of the components with the same frequency in the ZTs are extracted to compute the actual amplitude ratios.

♦ *Construction of faulty feeder detection criterion—–Online stage* 2

First, for any feeder j, the ratio of the standard amplitude ratio to the actual one is calculated and denoted as R_j. Second, the faulty feeder detection criterion is constructed as

$$\max_{1 \le j \le M} \left(R_j\right) \tag{12}$$

One can conclude from (12) that the maximum R_j corresponds to the actual faulty feeder.

It should be noted that all the measured ZTs are denoised by mathematical morphology (MM) [25] before using S-transform to extract the amplitudes of the frequency components. As shown in (2), the amplitudes of high frequency components (hundreds of kHz to MHz) attenuate more significantly than the lower ones. If the line length is long, high frequency components cannot be detected due to severe attenuation. According to Ref. [23], it can be known that the amplitude attenuation of traveling wave signal corresponds to a steep frequency band. In addition, the best frequency band of S-transform is 20 kHz ∼50 kHz [26]. To determine

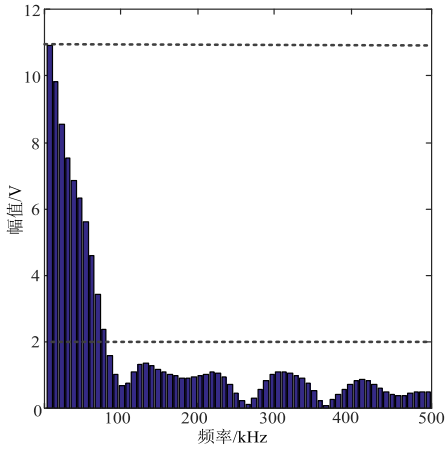

FIGURE 3. FFT spectrum of the ZT.

TABLE 1. Values of $\alpha_I^{(0)}$ corresponding to different frequencies.

Frequency	10kHz	20kHz	30kHz	40kHz	50kHz
$\alpha_i^{(0)}$ ($\times 10^{-6}$)	8.1333	15.252	22.155	28.812	35.255

an appropriate frequency component, the following points should be considered.

First, the FFT spectrum (amplitude-frequency characteristic) of the ZT when a fault occurs in the distribution feeder is computed and shown in Fig.3. It can be observed from the figure that most of the spectrum energy is concentrated in the low frequency band. The ratio of the amplitude of any high frequency component (>80 kHz) to that of the low frequency component (about 7.8 kHz) with the largest amplitude is smaller than 18.18%. To reduce computation error, the lower frequency components (<80 kHz) are more preferred than the higher ones (>80 kHz).

Second, it can be known that the core of faulty feeder detection lies in the difference between the amplitude ratios of the selected frequency components of the faulty and healthy feeders. Thus, the larger difference between the amplitudes of the frequency components in the ZTs acquired at both terminals of the distribution feeder is better when it comes to faulty feeder detection. According to eq. (11), the faulty feeder can be detected more reliably with the proposed criterion if the difference between R_{jm-kf} and R_{jm-jf} is more significant. Due to the fact that $R_{jm-jf} = 1$, the value of R_{jm-kf} should be far larger than 1. According to eq. (9), the value of R_{jm-kf} depends on $\alpha_i^{(0)}$ when the fault distance x_k and ρ_{k_st} determined by line parameters remain unchanged. The larger the value of $\alpha_i^{(0)}$, the larger the value of R_{jm-kf}. According to Ref. [26], $\alpha_i^{(0)}$ can be estimated by line constants solution module in PSCAD simulation. Table 1 lists the values of $\alpha_i^{(0)}$ corresponding to different frequencies. From the results, it can be observed that the value of $\alpha_i^{(0)}$ exceeds 10^{-5} when the frequency is equal to or larger than 20 kHz. The value of $\alpha_i^{(0)}$ grows with the increase of frequency. Thus, from this aspect, the lower frequency component (<20 kHz) is not recommended for faulty feeder detection.

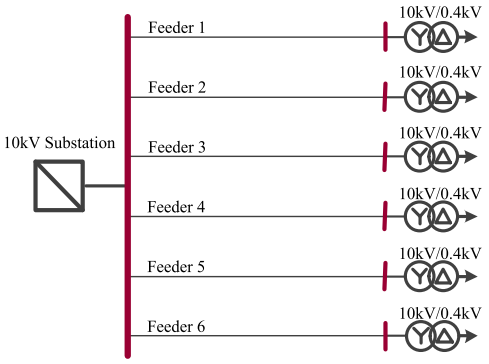

FIGURE 4. Diagram of the distribution network simulation model.

TABLE 2. Faulty feeder result with different frequencies.

Selected Frequency	20kHz	30kHz	40kHz	50kHz
Sampling Frequency	50kHz	70kHz	90kHz	110kHz
NC	98	97	96	97

Third, to select the most appropriate frequency from the frequency band 20 kHz ∼50 kHz, various faults have been simulated in the distribution network shown in Fig. 4 by PSCAD. The total number of the simulated faults is 100. Different fault resistances, inception angles, and distances are considered in these simulations. By extracting the amplitudes of the frequency components with 20, 30, 40, and 50 kHz, the faulty feeder detection results can be obtained by using the proposed method and shown in Table 2. NC in the table represents the total time of the correct faulty feeder detection in 100 fault events. According to Shannon sampling principle, the sampling frequency should be at least twice the bandwidth of the sampled frequency component. Thus, for each extracting frequency, the sampling frequency of the ZT measurement device is set as shown in the table. From the results, it can been seen that the accuracy of the faulty feeder detection with the four frequencies is almost the same. However, in actual field, the lower the sampling frequency, the lower the sampling cost. Thus, the frequency component with 20 kHz is selected for faulty feeder detection. Compared with traditional traveling wave methods whose sampling frequency can be as at least several hundreds of kHz, only 50 kHz sampling frequency is required in the proposed criterion.

IV. IMPLEMENTATION OF THE FAULTY FEEDER DETECTION CRITERION

From Fig.2, it can be seen that the amplitudes of the frequency components of the ZTs measured at both terminals of each feeder are extracted by S-transform and transmitted to the computing server equipped in substation. Thus, the key parts in implementation of the proposed faulty feeder detection criterion include: amplitude extraction by S-transform, signal length selection, and data communication. Details are described in the following subsections.

A. AMPLITUDE EXTRACTION BY S-TRANSFORM

The S-transform has many improved methods such as generalized S-transform, hyperbolic S-transform and so on. In the proposed method, the amplitude of the selected frequency component is simply used to construct the faulty feeder detection criterion. Only the basic S-transform (invented by Robert Glenn Stockwell in 1996) instead of the improved method is used. The MATLAB S-transform toolkit function is used to perform the basic S-transform. The toolbox function can be expressed by 'function $[C, T, F] = \mathrm{ST}\ (S, fmin, fmax, SR, FI)$'. In this function, the output variable C represents a complex matrix whose row and the column present the decomposition frequency and the time value. The other two output variables T and F represent two vectors containing the sampled time and frequency corresponding to each row of C. ST denotes the function name. The input parameters of the S-transform function are denoted as S, $fmin$, $fmax$, SR, and FI. S represents the signal to be decomposed by S-transform. $fmin$ and $fmax$ denote the minimum (Default $= 0$) and maximum (Default $=$ Nyquist scale) decomposition scales in the S-transform result. SR and FI are the time interval (Default $= 1$) between samples and the expected scale interval in the S-transform result (Default $= 1$).

To extract the expected amplitude of the selected frequency component, the parameters of S-transform needed to be set include $fmin$, $fmax$, SR, and FI. Since the amplitude of the frequency component with single frequency $\omega_i = 20$ kHz is utilized, thus the value of $fmin$ and $fmax$ should be equal. The sampling frequency is 50 kHz, thus the value of SR is 2×10^{-5} (s). FI remains the default value since there is no difference between $fmin$ and $fmax$. To select the appropriate value of $fmin$ (or $fmax$), the frequency corresponding to $fmin = 1$ (unit scale) should be firstly determined. Let $fmin = fmax = 1$, any element in the output vector F all equals to the frequency corresponding to unit scale. Since the increase of $fmin$ is linear, the value of $fmin$ can be then estimated by determining the decomposition scale corresponding to the required frequency. According to the above analysis, $fmin = fmax = 55$ in this manuscript.

B. SIGNAL LENGTH SELECTION CRITERIA

According to the basic propagation features of ZTs, the higher the frequency of the selected component, the larger the wave velocity of the component. In other words, the higher frequency components arrive more early at the measurement point than the lower ones. If the data window of the ZT is too short, the required frequency may not be contained. However, the implementation time of the proposed method may be long and the acquired signal may be mixed with too many steady-state components if the data window is too long. Thus, to ensure the extraction accuracy and reduce sampling time, an appropriate data window should be determined.

First, the determined data window must reflect a wave front shape. Second, the expected frequency ($\omega_i = 20$ kHz) must be included in the signal composed by the determined samples and low-frequency steady state components should not be included. According to the first criterion, the arrival time of the first wave front in the measured ZT should be

roughly determined, which can be easily realized by the current singularity detection algorithm. In this paper, the wavelet Teager energy algorithm (details are shown in [26]) is used to accomplish this task. Then, taking the determined arrival time as a benchmark, l_b and l_a samples before and after the benchmark is selected to combine the data window. Based on the second criterion, the spectrum of the samples whose length equals to l_a must contain the frequency close to the expected one. Let $l_a = 1, 2, \ldots,$ apply FFT to each data window, and find the frequency most close to 20 kHz. When $l_a < 10$, the expected frequency cannot be found. When $l_a = 10$, a component whose frequency is 19.992 kHz which is very close to 20 kHz. Thus, the minimum l_a is 10. Although the maximum of l_a cannot be determined, the minimum value is sufficient for calculation. In addition, the wave front of ZT is theoretically a step signal. To ensure the completeness of the wave front signal and continuity of the signal at the singularity point, the value of l_b can be far larger than l_a. In this paper, l_b is set as 100. Thus, the total length of the selected data window is 110 samples which corresponds to 2.2ms with 50 kHz sampling rate.

C. DATA COMMUNICATION

There are three types of data communications available to actual faulty feeder detection: power line carrier, optical fiber and GPRS communications. The reliability of the data communications mentioned above are briefly explained as follows.

(1) Optical fiber communication (OFC): light wave is the carrier of this type of communication and optical fiber is used as the transmission media, which contributes high reliability and transmission rate of this data communication. However, the construction cost of OFC is high, the erection of fiber optical is difficult, and repair work can be complex after a communication failure.

(2) Power line carrier communication (PCC): The principle of this communication is to modulate the data into high frequency signal at the transmitter and couple it at the receiver. PCC may be affected by transmission attenuation, noise interference and complex time variant features, which results in low reliability. However, the cost of this communication is low and repair work is easy.

(3) GPRS communication (GPRSC): GPRSC is based on wireless network and transmits data with packets. GPRSC has high reliability, network access speed, transmission rate, and network utilization efficiency and economy. The costs of GPRSC devices are low and installation of GPRS wireless units is convenient. The above features make GPRSC more applicable to the data communication between substation and terminal devices.

In actual field, OFC is only deployed in some critical occasions while GPRSC has been widely adopted in power distribution networks to realize reliable communication, which can meet the requirement of faulty feeder detection.

TABLE 3. Paramaters of the feeders in the system.

Type	Underground cables		
FN	1	2	5
L_F	6.8km	7.3km	4.9km
EP	PS		ZS
IM (Ω/m)	$0.3\times10^{-4}+j0.2\times10^{-3}$		$0.2\times10^{-3}+j0.2\times10^{-2}$
AD (S/m)	$j0.2\times10^{-7}$		$j0.2\times10^{-7}$
Type	Over-head Transmission Lines		
FN	3	4	6
L_F	9.5km	14km	8.2km
EP	PS		ZS
IM (Ω/m)	$0.3\times10^{-4}+j0.4\times10^{-3}$		$0.3\times10^{-3}+j0.1\times10^{-2}$
AD (S/m)	$j0.3\times10^{-8}$		$j0.2\times10^{-8}$

TABLE 4. Standard amplitud ratio of each feeder.

NGM	Standard Amplitude Ratios					
	FN=1	FN=2	FN=3	FN=4	FN=5	FN=6
UG	0.513	0.514	0.512	0.522	0.511	0.513
ASCG	0.513	0.513	0.512	0.522	0.511	0.513

V. SIMULATION EVALUATION

A 10 kV single-end radial distribution network shown in Fig.4 is established by PSCAD/EMTDC. The system consists of six feeders whose types, lengths, and parameters are listed in table 3. In the table, FN represents the feeder number, L_F denotes the line length, EP represents the electrical parameter, and IM and AD denote the impedance and admittance in per unit length of the feeder. PS and ZS represent positive and negative sequences. In the following tables, NGM denotes the neutral grounding mode. UG and ASCG represent ungrounded and arc-suppression coil grounded neutrals. The sampling frequency is set as 50 kHz.

Before conducting the online stage of the proposed faulty feeder detection criterion, a SPTEF is simulated at bus to conduct the offline stage. Figure 5 depicts the waveforms of the ZTs at both terminals in each feeder. In the figure, $U_{js}(j = 1, 2, \ldots, 6)$ and U_{je} in the legend represent the ZTs measured at starting and ending terminals of feeder j. Table 4 shows the standard amplitude ratio of the selected frequency component in the ZTs captured at both terminals of each feeder with different neutral grounding modes. It can be observed from table 4 that the standard amplitude ratio of each feeder in the ungrounded system is virtually identical to the one in arc-suppression coil grounded system.

A. CASE STUDY

In order to test the performance of the proposed criterion, three different SPTEFs are simulated in feeder 4 with different fault conditions. Detailed information of these fault cases are listed in Table 5 where FD represents the distance between the fault point and starting terminal of feeder 4. In each case,

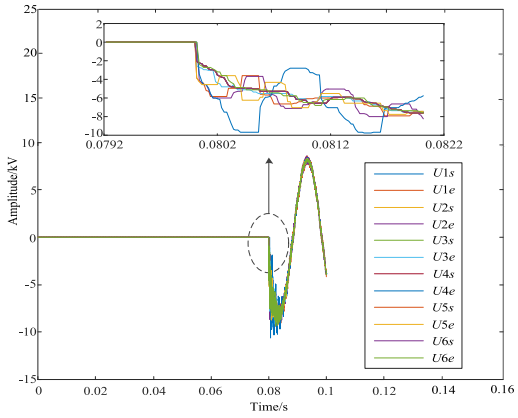

FIGURE 5. Waveforms of the measured ZTs when bus fault occurs.

TABLE 5. Fault information in each simulation case.

Case	NGM	FD	Fault impedance
①	UG	1.4km	10Ω
②	ASCG	6.9km	200Ω
③	ASCG	12.8km	10Ω

TABLE 6. Faulty feeder detection results in three cases.

Case		①	②	③
AAR	FN=1	0.511	0.490	0.516
	FN=2	0.514	0.490	0.517
	FN=3	0.510	0.491	0.518
	FN=4	0.104	0.106	0.106
	FN=5	0.509	0.514	0.514
	FN=6	0.511	0.519	0.519
R_{max}		5.019	4.925	4.925
Detected Faulty Feeder		Feeder 4	Feeder 4	Feeder 4

the actual amplitude ratio of the frequency component in the ZTs at both terminals of each feeder is extracted and displayed in Table 6. In the table, AAR denotes the actual amplitude ratios. The maximum ratio of the standard amplitude ratio to the actual one is also listed and denoted as R_{max} in the table. From table 4 and 6, it can be concluded that the actual amplitude ratios of the sound feeders are close to the standard ones. However, there exists a significant difference between the amplitude ratio of feeder 4 in bus fault and that in feeder 4 fault. According to the results in table 6, it can be observed that the proposed criterion can effectively detect the faulty feeder.

B. SENSITIVITY ANALYSIS

1) EFFECTS OF NEUTRAL GROUNDING MODES AND FAULT CONDITIONS

In order to investigate the effects of neutral grounding modes and fault conditions, the SPTEFs with different fault impedances and inception angles is simulated in feeder 1 and feeder 6 with grounded and arc-suppression

TABLE 7. Three different fault conditions.

FFD	FCN	I_F	θ_F	FD
Feeder 6	1	10Ω	90°	5.3km
	2	10Ω	30°	2.1km
	3	200Ω	30°	1.4km

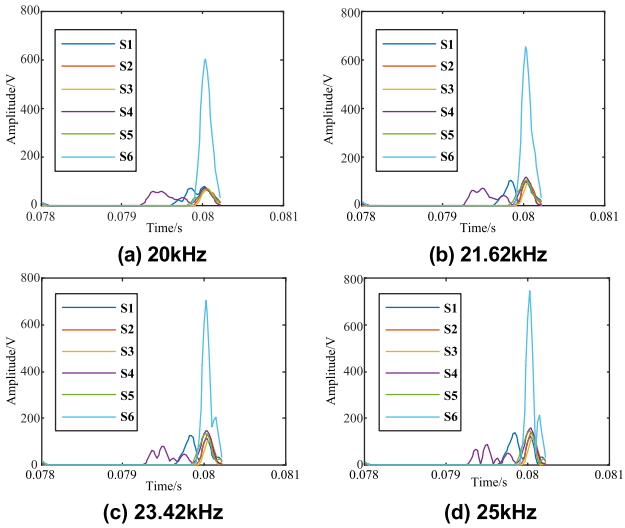

FIGURE 6. S-transform time-frequency amplitude curve of each feeder in fault condition 1.

grounded neutrals. The S-transform results of the ZTs with 20∼25kHz at both terminals of each feeder with three different fault conditions (Shown in Table 7) are depicted in Fig.6, 7, and 8. In the table, FCN denotes the fault condition number. In the three figures, S1, S2, . . . , S6 in the legend represent the S-transform amplitude curves of the frequency components in the ZTs at the ending terminal of feeder 1, 2, . . . , 6. It can be observed from the figures that the S-transform amplitude curve varies with the fault condition and extraction frequency. In addition, the faulty feeder corresponds to the maximum amplitude of all the time-frequency curves, which can be a significant difference between the faulty and healthy feeders.

Table 8 presents the faulty feeder detection results. In the table, FFD and FFDR denote the actual faulty feeder and faulty feeder detection result. I_F and θ_F represent the fault impedance and inception angle. In each row of the last column, the first real number is R_{max}. Although the maximum ratio of the standard amplitude ratio to the actual one is different with different neutral and fault conditions, it always corresponds to the actual faulty feeder. The results in table 8 show that the proposed criterion is independent from neutral grounding modes and fault conditions.

2) EFFECTS OF HIGH-IMPEDANCE FAULTS

In actual distribution network, high-impedance fault (HIF) is a special and worrisome fault case that appears, for example, when the feeder conductor makes electrical contact with poorly grounded objects [27]. In this section, the performance of the proposed criterion is validated by simulating the HIFs

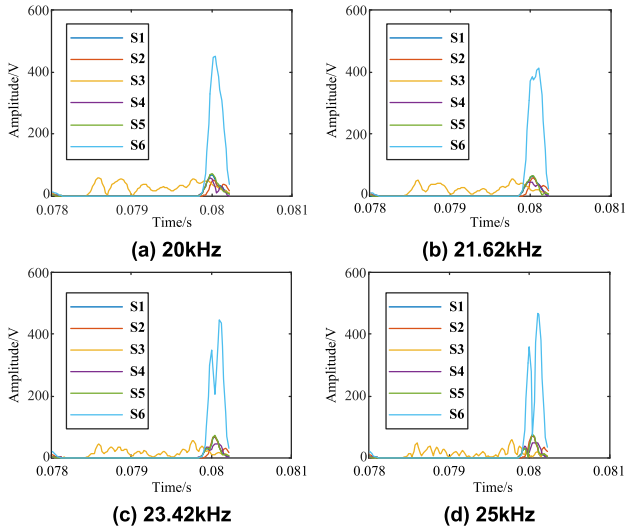

FIGURE 7. S-transform time-frequency amplitude curve of each feeder in fault condition 2.

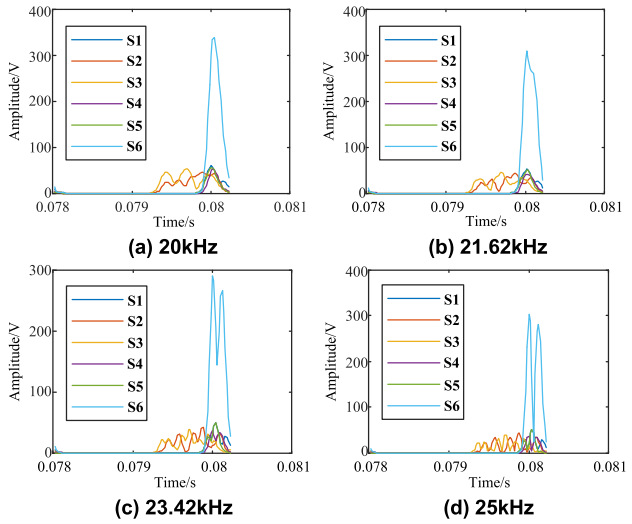

FIGURE 8. S-transform time-frequency amplitude curve of each feeder in fault condition 3.

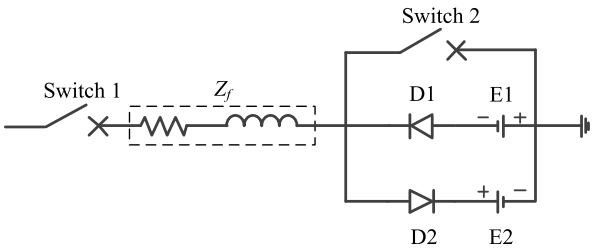

FIGURE 9. Integrated high-impedance fault simulation model.

in a distribution feeder. The SPTEFs with constant high impedance and nonlinear impedance (whose parameters are shown in [28]) are considered in one simulation model shown in Fig.9. In the figure, switch 1 controls the inception time of the HIF and the state of the switch 2 determines the type of the HIF. Z_f is a fixed impedance. D1 and D2 represent

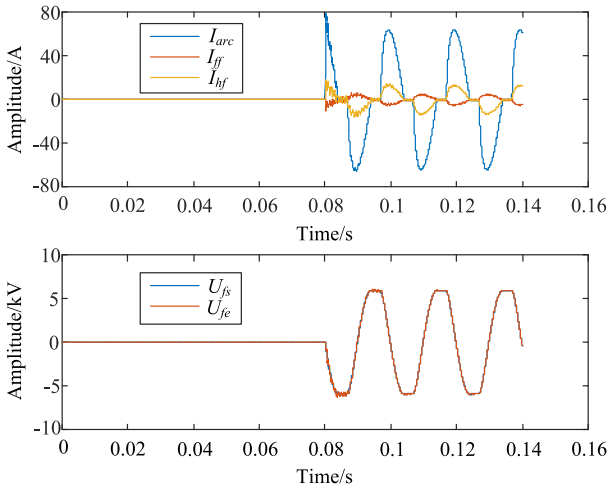

FIGURE 10. HIFNI current, zero-mode currents and ZTs in ungrounded system.

TABLE 8. Faulty feeder detection results with different neutrals and fault conditions.

FFD	NGM	I_F	θ_F	FD	FFDR
Feeder 1	UG	200Ω	30°	0.8km	4.188, Feeder 1
			90°	5.3km	4.257, Feeder 1
		10Ω	30°	2.1km	4.227, Feeder 1
			90°	4.5km	4.502, Feeder 1
	ASCG	200Ω	30°	0.8km	4.213, Feeder 1
			90°	5.3km	4.324, Feeder 1
		10Ω	30°	2.1km	4.316, Feeder 1
			90°	4.5km	4.625, Feeder 1
Feeder 6	UG	200Ω	30°	0.8km	4.958, Feeder 6
			90°	5.3km	4.971, Feeder 6
		10Ω	30°	2.1km	4.898, Feeder 6
			90°	4.5km	4.976, Feeder 6
	ASCG	200Ω	30°	1.4km	4.788, Feeder 6
			90°	6.7km	4.835, Feeder 6
		10Ω	30°	3.6km	4.683, Feeder 6
			90°	5.5km	4.792, Feeder 6

two antiparallel diodes. E1 and E2 are two antiparallel DC voltage sources. The following two HIF simulation cases are investigated: (1) Switch 1 and Switch 2 are all closed. HIFs with fixed impedances (HIFFIs) are simulated at three different locations in feeder 4; (2) Switch 1 is closed but switch 2 is open. HIFs with nonlinear impedances (HIFNIs) are simulated in feeder 2, 3, and 5.

Figure 10 displays the HIFNI current and ZTs in the ungrounded system. Figure 11 depicts the HIFNI current, zero-mode currents and ZTs in the arc-suppression coil grounded systems. In the figure, I_{arc} represents the HIFNI current. I_{ff} and I_{hf} denote the zero-mode currents at starting terminals of the faulty and sound feeders. U_{fs} and U_{fe} represent the ZTs at starting and ending terminals of the faulty feeder. As shown in Fig.10 and Fig.11, the zero-mode currents of the faulty and sound feeders when HIFNI occurs in ungrounded system are almost in opposite polarity. However, they are almost in the same direction when HIFNI occurs in arc-suppression coil grounded system, which makes it difficult to detect the faulty feeder by the steady-state

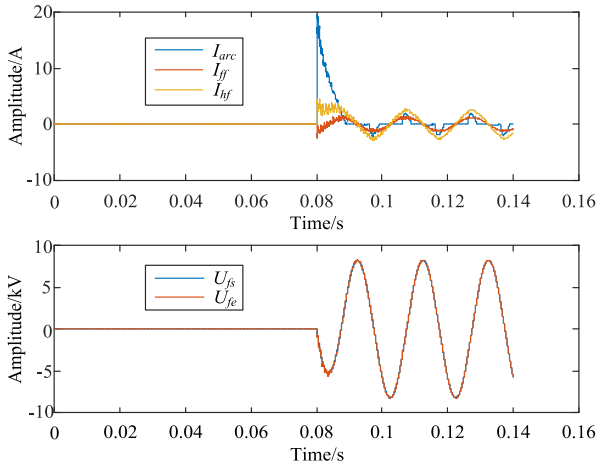

FIGURE 11. HIFNI current, zero-mode currents and ZTs in arc-suppression coil grounded system.

TABLE 9. Faulty feeder detection results in case 1.

FD		2.2km		7.7km		13.1km	
I_F		2kΩ	3kΩ	2kΩ	3kΩ	2kΩ	3kΩ
AAR	FN=1	0.511	0.510	0.495	0.496	0.451	0.452
	FN=2	0.511	0.511	0.494	0.495	0.449	0.448
	FN=3	0.510	0.511	0.496	0.496	0.451	0.451
	FN=4	0.104	0.104	0.103	0.103	0.093	0.093
	FN=5	0.515	0.512	0.497	0.496	0.451	0.451
	FN=6	0.511	0.511	0.495	0.494	0.450	0.451
FFDR		5.036	5.036	5.055	5.055	5.643	5.643
		Feeder 4					

TABLE 10. Faulty feeder detection results in case 2.

FFD		Feeder 2	Feeder 3	Feeder 5
FD		2.5km	6.7km	4.6km
AAR	FN=1	0.511	0.509	0.511
	FN=2	0.132	0.509	0.509
	FN=3	0.509	0.104	0.513
	FN=4	0.512	0.510	0.509
	FN=5	0.508	0.507	0.131
	FN=6	0.511	0.509	0.510
FFDR		3.894, Feeder 2	4.899, Feeder 3	3.901, Feeder 5

methods. In addition, the features of the HIFNI current are: buildup, shoulder, nonlinearity, and asymmetry. Table 9 and Table 10 list the faulty feeder detection results in case 1 and 2, respectively. From the tables, it can be seen that the proposed criterion can effectively detect the faulty feeder when the HIF occurs in power distribution network.

3) EFFECTS OF NOISES

In actual field, the measured ZTs are susceptible to noises. To investigate the effects of noises on the proposed criterion, the Gaussian white noises with different signal-to-noise ratios (SNRs) are added into the measured ZTs after simulating a HIFNI in feeder 1. By applying MM, the de-noised signals are acquired. Figure 12 illustrates the noise-contaminated and de-noised ZTs at both terminals of the faulty feeders with

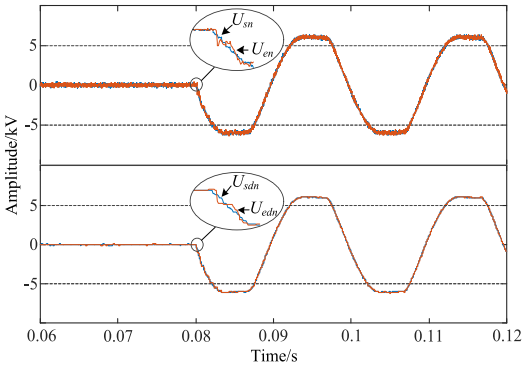

FIGURE 12. Noise-contaminated and de-noised ZTs of the faulty feeder.

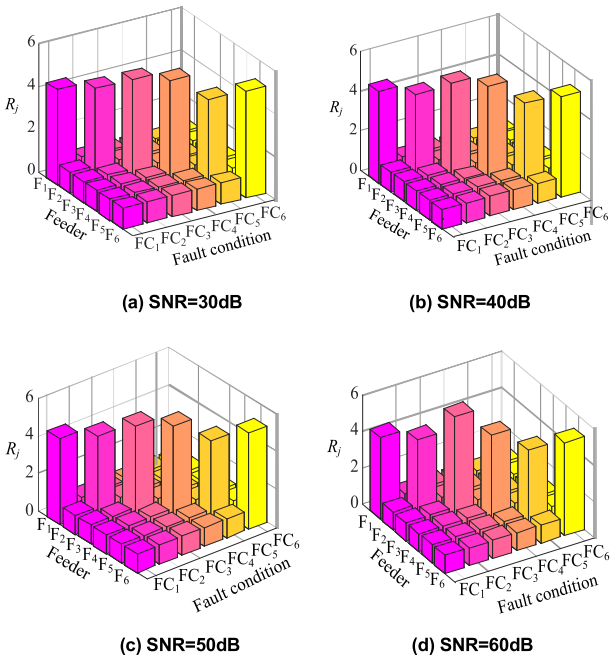

FIGURE 13. Rj of each feeder with different SNR values of noises.

SNR = 30dB. In the figure, U_{sn} and U_{en} represent the ZTs with noises. U_{sdn} and U_{edn} denote the de-noised ZTs. The ratios of the standard amplitude ratios to the actual ones for each feeder with different SNR values of the noises are presented in Fig.13. In the figure, F_j and R_j represent feeder j and the ratio of the standard amplitude ratio to the actual one of feeder j. The symbol meanings of the ordinates in each subfigure are listed in Table 11. In the table, OF denotes an ordinary SPTEF. It can be clearly observed from Fig.13 that the number of the actual faulty feeder always corresponds to the maximum value of R_j despite of SNR values of noises in a certain range. Thus, the proposed criterion is not affected by the noises to some extent.

To show the performance of the method when the noise intensity gets very large, a single-phase-to-earth fault (fault condition: FC_2 in Table 11) is simulated with SNR = 5dB. By using the de-noised ZTs at both terminals of each feeder, the faulty feeder detection result in this case is listed in Table 12.

TABLE 11. Symbol meanings of the ordinates.

Symbol	FC_1	FC_2	FC_3
Meaning	OF FN=1 FD=0.6km I_F=200Ω	HIFNI FN=2 FD=5.5km	OF FN=3 FD=3.7km I_F=10Ω
Symbol	FC_4	FC_5	FC_6
Meaning	HIFFI FN=4 FD=11.2km I_F=3000Ω	OF FN=5 FD=2.3km I_F=100Ω	HIFNI FN=6 FD=7.6km

TABLE 12. Faulty feeder detection result with snr = 5dB.

FN	FN=1	FN=2	FN=3	FN=4	FN=5	FN=6	FFDR
SAR	0.513	0.514	0.512	0.522	0.511	0.513	
AAR	0.837	0.501	0.526	0.924	0.932	1.191	Feeder 2
RSA	0.613	**1.026**	0.973	0.565	0.548	0.431	

TABLE 13. Parameters of the two cables.

Cable Number	Type	EP	PS	ZS
Cable 1	YJV22-6/10kV-3×95	IM (Ω/m)	$0.38\times10^{-4}+j0.17\times10^{-3}$	$0.26\times10^{-3}+j0.18\times10^{-2}$
		AD (S/m)	$j0.2\times10^{-7}$	$j0.24\times10^{-7}$
Cable 2	YJV22-8.7/10kV-3×70	IM (Ω/m)	$0.42\times10^{-4}+j0.19\times10^{-3}$	$0.27\times10^{-3}+j0.22\times10^{-2}$
		AD (S/m)	$j0.22\times10^{-7}$	$j0.26\times10^{-7}$

In the table, SAR represents the standard amplitude ratio of the ZTs at both terminals of a feeder. RSA is the ratio of SAR to AAR. From the table, it can be observed that the faulty feeder can be still correctly identified by using the maximum ratio between the standard and actual amplitude ratios. It should be noted that the difference between the six ratios of SARs to AARs is not significant in this case. In other words, when SNR is very small, the calculated maximum ratio of SAR to AAR does not exceed the other ones by too much although the faulty feeder can be still detected. Considering the sampling error in actual field, the faulty feeder detection may be wrong in this extreme case.

4) EFFECTS OF MIXED FEEDERS

To verify the effectiveness of the proposed method in mixed feeders, a case where two connected cables with different parameters in feeder k is analyzed. Table 13 lists the electrical parameters of the two cables. In theory, the proposed method is not affected by the mixed feeder. Detailed analysis is shown in Appendix *B*. In simulation, feeder 4 in the constructed distribution network model is replaced by a mixed feeder with the two cables. Two single-phase-to-earth faults are simulated in the two cables of feeder 4. The faulty feeder detection results by the proposed method are shown in Table 14. In the table, FC represents the faulty cable. From the table, it can be seen that the method can correctly identify the faulty feeder in this case.

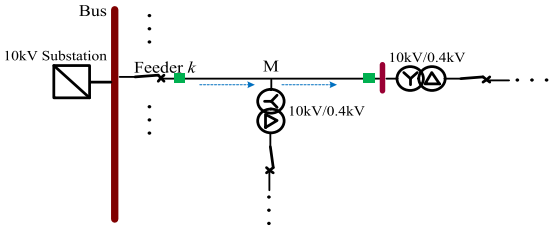

FIGURE 14. Branch line connects to feeder *k*.

5) EFFECTS OF LOW-VOLTAGE BRANCH LINES

In actual field, 0.4kV branch line may connected to different locations of a distribution feeder rather than to the end of the feeder. As shown in Fig.14 below, a 0.4kV branch line comes from point M of feeder k.

In theory, when the ZT propagates to the connection point M, it will reflect and refract. As for frequency ω_i, the equivalent wave impedance Z_{eq_i} of the feeder at right side of M and the branch transformer can be expressed by

$$Z_{eq\_i} = \frac{Z_{1\_i} \cdot Z_{T\_i}}{Z_{1\_i} + Z_{T\_i}} \tag{13}$$

where Z_{1_i} and Z_{T_i} represent the wave impedances of the feeder at right side of M and the branch transformer. As for the ZTs, the wave impedance of transformer can be regarded to be infinite. Thus, we have

$$Z_{eq\_i} = Z_{1\_i} \tag{14}$$

According to the definition of reflection and refraction coefficients, we have

$$\begin{cases} \rho_{u\_i} = 0 \\ \gamma_{u\_i} = 1 \end{cases} \tag{15}$$

In (15), ρ_{u_i} and γ_{u_i} are the reflection and refraction coefficients when the ZT propagates from left side to the right side of point M. It is evident that there is no reflection of the ZT and the refraction has no effect on the ZT at point M. Thus, the proposed method is still effective in this case.

6) EFFECTS OF DISTRIBUTED LINE PARAMETERS

The initial amplitude of the fault-generated ZT at the fault point is independent from distribution line parameters since it is only dependent on fault conditions and system voltage. However, when the ZT propagates along the line, its amplitude depends on the distribution line parameters. The amplitude of the component with ω_i in the ZT at the point x away from the fault location is

$$\left|U_i^{(0)}(x)\right| = e^{-\alpha_i^{(0)}x} \cdot \frac{A}{\omega_i} \tag{16}$$

In the above equation, $\alpha_i^{(0)}$ is the real part of the zero-mode propagation constant which reflects the amplitude attenuation degree of the ZTs. The value of $\alpha_i^{(0)}$ can be calculated by

$$\alpha_i^{(0)} = \sqrt{\frac{1}{2}\left[R_0G_0 - \omega_i^2 L_0C_0 + \sqrt{\left(L_0^2 + \omega_i^2 L_0^2\right)\left(G_0^2 + \omega_i^2 C_0^2\right)}\right]} \tag{17}$$

TABLE 14. Faulty feeder detection results with mixed feeder.

FC	FD (km)	FN	FN=1	FN=2	FN=3	FN=4	FN=5	FN=6	FFDR
		SAR	0.47	0.476	0.534	0.616	0.7	0.698	
Cable 1	2.5	AAR	0.546	0.56	0.533	0.294	0.519	0.609	Feeder 4
		Ratio of ASR to AAR	0.861	0.85	1.002	**2.093**	1.349	1.146	
Cable 2	10.3	AAR	0.574	0.41	0.49	0.211	0.53	0.485	Feeder 4
		Ratio of SAR to AAR	0.82	1.16	1.09	**2.914**	1.32	1.441	

TABLE 15. A comparison between the proposed method and some other methods.

Methods	Noises	HIFFIs	HIFNIs	Training	Threshold	IT (ms)	NC
[5]	Not Considered	Considered	Not Considered	Not Required	Not Required	6.04	88
[7]	Not Considered	Considered	Not Considered	Not Required	Required	7.66	84
[10]	Not Considered	Considered	Not Considered	Not Required	Required	5.72	82
[13]	Not Considered	Considered	Not Considered	Not Required	Required	7.91	83
[19]	Not Considered	Considered	Not Considered	Not Required	Not Required	2.13	85
[20]	Not Considered	Not Considered	Considered	Not Required	Not Required	3.58	81
[21]	Considered	Considered	Considered	Required	Not Required	8.46	93
[22]	Not Considered	Not Considered	Not Considered	Required	Not Required	9.31	86
Proposed one	Considered	Considered	Considered	Not Required	Not Required	1.25	98

where R_0, L_0, G_0 and C_0 are the zero-mode resistance, inductance, conductance, and capacitance in per unit length of the feeder. It can be observed from (16) and (17) that the amplitude of the ZT depends on the distribution line parameters.

As shown in the manuscript, the standard amplitude ratio AP_{jm} can be expressed by

$$AP_{jm} = \frac{\left|U^{(0)}_{jm\_st}\right|}{\left|U^{(0)}_{jm\_ed}\right|} = \frac{1}{\left|\rho_{j\_ed}\right|} \cdot e^{\alpha_i^{(0)} L_j} \tag{18}$$

where ρ_{j_ed} is the reflection coefficient at ending terminal. From (17) and (18), it is clear that the standard amplitude depends on the line electrical parameters. If the cables in power distribution network are changed for examination and repair, the standard amplitude ratio should be constructed again since the parameters of the new cables may be different from those of the old ones.

7) DISCUSSION ON EFFECTIVENESS OF THE METHOD WITH ONLY ONE-END DATA

In the proposed method, it can be observed that the transients measured at both terminals of the feeders are needed. If the measurements at the ending terminal of the feeders are not available, the method will be inadequate for the purpose of faulty feeder detection. However, in China, the measurement devices are usually equipped at the high-voltage side of the 10kV/0.4kV transformers in modern distribution networks. Thus, the case where the measurements at the ending terminals are not available is rare in smart grids. In addition, strict synchronization is not required since only the amplitude of the transient is utilized though the measurements at both ends of the feeders are indispensable.

8) DISCUSSION ON DATA COMMUNICATION DELAY

The average communication propagation delay T_d can be expressed by

$$T_d = \frac{2d_s \cdot M}{v_{avg}} \tag{19}$$

where ds is the size of the data recorded at each measurement point. M represents the total number of the distribution feeders. vavg denotes the average data transmission speed. Taken the simulation data as an example, the size of the data is about 0.05 KB, M equals to six, and vavg can reach as 60 KB/s. Thus, the average data communication delay is close to 10ms. The implementation time of the proposed method is about 1.25ms. The total time of a faulty feeder detection by using the proposed method can be 11.25ms. At this time, the circuit-breakers do not operate. Thus, the data communication delay has little effect on the reliability of the method.

C. COMPARISON WORK

A comparison between the proposed method and some other methods is conducted to show the advantages of the proposed method. The results are listed in Table 15 below. In the table, IT represents the implementation time of the faulty feeder detection methods. NC denotes the total time of correct faulty feeder detection of each method with 100 different fault cases (with different noise levels, HIFs, or fault conditions). All the computations were carried out in a computer whose processor is Intel Core(TM) i5-6300HQ @ 2.30 GHz.

It can be clearly observed in the comparison result in Table 15 that the proposed method has the following advantages. First, it considers the noise effect which is a very important factor in actual field. From the simulation, the proposed method can be still effective even with 30dB noise. However, most of the methods [5], [7], [10], [13], [19], [20], [22]

cannot work with such noise. Second, the proposed method is verified to be not affected by HIFs which commonly occur in the feeder when the feeder conductor makes electrical contact with poorly grounded objects. However, most of the methods [5], [7], [10], [13], [19], [20], [22] do not consider this type of fault. Third, the methods in [21], [22] may require a large data set to be trained by neural network, which adds to the time and cost and reduces the feasibility of actual-field practice, while the proposed one does not. Fourth, the methods in [7], [10] and [13] require to set some key parameters in the criterion of faulty feeder detection, which clearly limits the application of these methods. Nevertheless, the proposed method does not need to set any key parameters in implementation of the faulty feeder criterion. It can be seen the proposed method has the least implementation time. In addition, compared with the others, the proposed one has the highest accuracy.

VI. CONCLUSION

This paper constructs a novel and reliable faulty feeder detection criterion by using the amplitude ratio of the ZTs measured at both terminals of each feeder. The proposed criterion does not require strict synchronization and high sampling frequency. Various fault simulations have been conducted by PSCAD/EMTDC. Main conclusions are as follows:

First, the amplitude ratio of the ZTs at both ends of each feeder is irrelevant to the initial fault conditions and neutral grounding modes of the system.

Second, there exists a difference between the amplitude ratio of the ZTs measured in the faulty feeder and those of the sound feeders in bus and feeder faults, which can be used to construct a new faulty feeder detection criterion.

Third, substantial simulation results show that the proposed criterion is not affected by neutral grounding modes, fault conditions, high impedance faults and noises.

APPENDIX

A. REFLECTION COEFFICIENT

When the transients propagate along a feeder line, the reflection and refraction will occur if the wave impedance suddenly changes at point M as shown in Fig.A1.

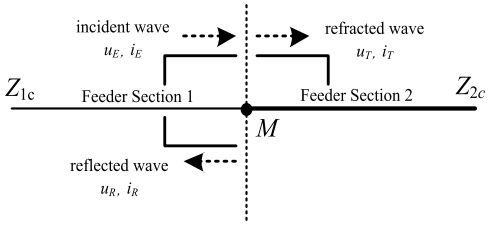

FIGURE A1. Reflection and refraction of the transients at point M.

In the figure, $Z_{1\,c}$ and $Z_{2\,c}$ are the wave impedances of feeder section 1 and 2, respectively. u_E and i_E denote the incident voltage and current transients. u_T and i_T represent the refracted voltage and current transients. u_R and i_R are the reflected voltage and current transients. At point M, the following relationships can be obtained:

$$\begin{cases} u_T = u_E + u_R \\ i_T = i_E + i_R \end{cases} \tag{A1}$$

At the same time, we have:

$$\begin{cases} u_T = i_T \cdot Z_{2c} \\ u_R = -i_R \cdot Z_{1c} \\ u_E = i_E \cdot Z_{1c} \end{cases} \tag{A2}$$

By rearranging eq. (A1) and eq. (A2), we have:

$$\begin{cases} u_R = \dfrac{Z_{2c} - Z_{1c}}{Z_{2c} + Z_{1c}} \cdot u_E = \rho_u \cdot u_E \\ u_T = \dfrac{2Z_{2c}}{Z_{2c} + Z_{1c}} \cdot u_E = \gamma_u \cdot u_E \end{cases} \tag{A3}$$

where ρ_u and γ_u are defined as the reflection and refraction coefficients and expressed by

$$\begin{cases} \rho_u = \dfrac{Z_{2c} - Z_{1c}}{Z_{2c} + Z_{1c}} \\ \gamma_u = \dfrac{2Z_{2c}}{Z_{2c} + Z_{1c}} \end{cases} \tag{A4}$$

B. EFFECTS OF MIXED FEEDERS

The lengths of the two cables are denoted as L_1 and L_2. The wave impedances of the two cables are written as Z_1 and Z_2. In this case, the ZT propagation is shown in Fig. A2.

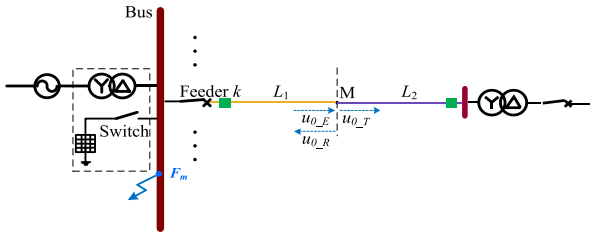

FIGURE A2. Diagram of ZT propagation in mixed feeder k.

In the figure, it can be observed that the ZT reflects and refracts at the connection point M. u_{0_E}, u_{0_R} and u_{0_T} represent the incident, reflected and refracted ZTs. The attenuation coefficients of the two cables with ω_i are denoted as $\alpha_1^{(0)}$ and $\alpha_2^{(0)}$. The refraction coefficient of the ZT propagates from cable 1 to cable 2 is presented as γ_{12} and that of the ZT propagates in the opposite direction is denoted as γ_{21}. If the fault occurs at bus, the standard amplitude ratio AP can be expressed by

$$\begin{cases} AP = \dfrac{1}{|\rho_{ed}|} e^{\alpha_1^{(0)} L_1} e^{\alpha_2^{(0)} L_2} \dfrac{1}{|\gamma_{12}|} \\ \gamma_{12} = \dfrac{2Z_2}{Z_1 + Z_2} \end{cases} \tag{A5}$$

When the fault occurs in cable 1, the actual amplitude ratio AP_{k1} is

$$AP_{k1} = \frac{|\rho_{k\_st}|}{|\rho_{k\_ed}|} e^{\alpha_1^{(0)}(L_1 - 2x)} e^{\alpha_2^{(0)} L_2} \tag{A6}$$

Thus, the ratio of AP to AP_{k1} is

$$R_1 = \frac{1}{|\rho_{st}|} e^{2\alpha_1^{(0)} x} > 1 \tag{A7}$$

When the fault occurs in cable 2, the actual amplitude ratio AP_{k2} is

$$\begin{cases} AP_{k2} = \dfrac{|\rho_{st}|}{|\rho_{ed}|} e^{\alpha_2^{(0)}(L_2-2x)} e^{-\alpha_1^{(0)} L_1} |\gamma_{21}| \\ \gamma_{21} = \dfrac{2Z_1}{Z_1+Z_2} \end{cases} \tag{A8}$$

Thus, the ratio of AP to AP_{k2} is

$$R_2 = \frac{1}{|\rho_{st}|} e^{2\alpha_2^{(0)} x} e^{2\alpha_1^{(0)} L_1} \frac{|\gamma_{12}|}{|\gamma_{21}|} \tag{A9}$$

The wave impedance of cable 1 is almost equal to that of cable 2. Thus, $|\gamma_{12}| \approx |\gamma_{21}|$ and $R_2 > 1$.

REFERENCES

[1] M. Shafiullah and M. A. Abido, "S-transform based FFNN approach for distribution grids fault detection and classification," *IEEE Access*, vol. 6, pp. 8080–8088, 2018.
[2] K. Zhu, P. Zhang, W. Wang, and W. Xu, "Controlled closing of PT delta winding for identifying faulted lines," *IEEE Trans. Power Del.*, vol. 26, no. 1, pp. 79–86, Feb. 2011.
[3] W. Wang, K. Zhu, P. Zhang, and W. Xu, "Identification of the faulted distribution line using thyristor-controlled grounding," *IEEE Trans. Power Del.*, vol. 24, no. 1, pp. 52–60, Jan. 2009.
[4] X. Lin, J. Huang, and S. Ke, "Faulty feeder detection and fault self-extinguishing by adaptive petersen coil control," *IEEE Trans. Power Del.*, vol. 26, no. 2, pp. 1290–1291, Apr. 2011.
[5] B. Liu, H. Ma, H. Xu, and P. Ju, "Single-phase-to-ground fault detection with distributed parameters analysis in non-direct grounded systems," *CSEE J. Power Energy Syst.*, to be published.
[6] K. Sarwagya, S. De, and P. K. Nayak, "High-impedance fault detection in electrical power distribution systems using moving sum approach," *IET Sci., Meas. Technol.*, vol. 12, no. 1, pp. 1–8, Jan. 2018.
[7] M. F. Abdel-Fattah and M. Lehtonen, "Transient algorithm based on earth capacitance estimation for earth-fault detection in medium-voltage networks," *IET Gener., Transmiss. Distrib.*, vol. 6, no. 2, pp. 161–166, Feb. 2012.
[8] K. Pandakov, H. K. Høidalen, and S. Trætteberg, "An additional criterion for faulty feeder selection during ground faults in compensated distribution networks," *IEEE Trans. Power Del.*, vol. 33, no. 6, pp. 2930–2937, Dec. 2018.
[9] Y. Wang, Y. Huang, X. Zeng, G. Wei, J. Zhou, T. Fang, and H. Chen, "Faulty feeder detection of single phase-earth fault using grey relation degree in resonant grounding system," *IEEE Trans. Power Del.*, vol. 32, no. 1, pp. 55–61, Feb. 2017.
[10] X. Lin, S. Ke, Y. Gao, B. Wang, and P. Liu, "A selective single-phase-to-ground fault protection for neutral un-effectively grounded systems," *Int. J. Electr. Power Energy Syst.*, vol. 33, no. 4, pp. 1012–1017, May 2011.
[11] T. Henriksen, "Faulty feeder identification in high impedance grounded network using charge–voltage relationship," *Electr. Power Syst. Res.*, vol. 81, no. 9, pp. 1832–1839, Sep. 2011.
[12] Z. Zhixia, L. Xiao, and P. Zailin, "Fault line detection in neutral point ineffectively grounding power system based on phase-locked loop," *IET Gener., Transmiss. Distrib.*, vol. 8, no. 2, pp. 273–280, Feb. 2014.
[13] X. Lin, J. Sun, I. Kursan, Z. Li, X. Li, and D. Yang, "Zero-sequence compensated admittance based faulty feeder selection algorithm used for distribution network with neutral grounding through Peterson-coil," *Int. J. Electr. Power Energy Syst.*, vol. 63, pp. 747–752, Dec. 2014.
[14] N. Suo, C. Zhang, and S. Wang, "Fault line selection in the non-solid earthed network based on the model identification method," *Autom. Electr. Power Syst.*, vol. 28, no. 19, pp. 65–70, 2004.
[15] P. Liu and C. Huang, "Detecting single-phase-to-ground fault event and identifying faulty feeder in neutral ineffectively grounded distribution system," *IEEE Trans. Power Del.*, vol. 33, no. 5, pp. 2265–2273, Oct. 2018.
[16] M. A. Barik, A. Gargoom, M. A. Mahmud, M. E. Haque, H. Al-Khalidi, and A. M. T. Oo, "A decentralized fault detection technique for detecting single phase to ground faults in power distribution systems with resonant grounding," *IEEE Trans. Power Del.*, vol. 33, no. 5, pp. 2462–2473, Oct. 2018.
[17] M. Loos, S. Werben, M. Kereit, and J.-C. Maun, "Fault direction method in compensated network using the zero sequence active energy signal," in *Proc. Eurocon*, Zagreb, Croatia, 2013, pp. 717–723.
[18] L. Pan, Y. Ping, and F. Yu, "Fault line selection in non-solidly earthed network based on phase-frequency characteristic and multi-frequency band analysis," *Autom. Electr. Power Syst.*, vol. 31, no. 4, pp. 76–79 and 84, 2007.
[19] X. Dong and S. Shi, "Identifying single-phase-to-ground fault feeder in neutral noneffectively grounded distribution system using wavelet transform," *IEEE Trans. Power Del.*, vol. 23, no. 4, pp. 1829–1837, Oct. 2008.
[20] X. Dong, J. Wang, S. Shi, B. Wang, B. Dominik, and M. Redefern, "Traveling wave based single-phase-to-ground protection method for power distribution system," *CSEE J. Power Energy Syst.*, vol. 1, no. 2, pp. 75–82, Jun. 2015.
[21] M.-F. Guo, X.-D. Zeng, D.-Y. Chen, and N.-C. Yang, "Deep-learning-based earth fault detection using continuous wavelet transform and convolutional neural network in resonant grounding distribution systems," *IEEE Sensors J.*, vol. 18, no. 3, pp. 1291–1300, Feb. 2018.
[22] T. Ji, Q. Pang, and X. Liu, "Study on fault line detection based on genetic artificial neural network in compensated distribution system," in *Proc. IEEE Int. Conf. Inf. Acquisition*, Weihai, China, Aug. 2006, pp. 1427–1431.
[23] M. Xu, L. Xu, and L. Lin, "A fault location method for the single-phase-to-earth fault in distribution system based on the attenuation characteristic of zero-mode traveling wave," *Trans. China Electrotech. Soc.*, vol. 30, no. 14, pp. 397–404, 2015.
[24] J. Wang, X. Dong, and S. Shi, "Traveling wave transmission research for overhead lines of radial distribution power systems considering frequency characteristics," *Proc. CSEE*, vol. 33, no. 22, pp. 96–102, 2013.
[25] N. Peng, L. Zhou, R. Liang, and H. Xu, "Fault location of transmission lines connecting with short branches based on polarity and arrival time of asynchronously recorded traveling waves," *Electr. Power Syst. Res.*, vol. 169, pp. 184–194, Apr. 2019.
[26] P. Nan, C. Menghan, L. Rui, and F. Zare, "Asynchronous fault location scheme for half-wavelength transmission lines based on propagation characteristics of voltage travelling waves," *IET Gener., Transmiss. Distrib.*, vol. 13, no. 4, pp. 502–510, Feb. 2019.
[27] R. G. Ferraz, L. U. Iurinic, and A. D. Filomena, "Arc fault location: A nonlinear time varying fault model and frequency domain parameter estimation approach," *Int. J. Elect. Power Energy Syst.*, vol. 80, pp. 347–355, Sep. 2016.
[28] L. U. Iurinic, A. R. Herrera-Orozco, and R. G. Ferraz, "Distribution systems high-impedance fault location: A parameter estimation approach," *IEEE Trans. Power Del.*, vol. 31, no. 4, pp. 1806–1814, Aug. 2016.

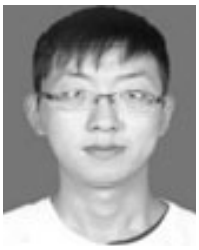

NAN PENG (S'18) received the B.S. degree in electrical engineering from Shandong University, Jinan, China, in 2015. He is currently pursuing the Ph.D. degree in electrical engineering with the China University of Mining and Technology, Xuzhou, China. His current research interests include power system protection and application of signal and information processing in power systems.

KAI YE received the B.S. degree in electrical engineering from Hangzhou Dianzi University, Hangzhou, China, in 2017. He is currently pursuing the M.S. degree with the China University of Mining and Technology, Xuzhou, China. His current research interests include electromagnetic transient analysis in power systems and power system protection.

RUI LIANG (M'14) received the B.Sc. and Ph.D. degrees from the Department of Electrical Engineering, China University of Mining and Technology, in 2001 and 2010, respectively. Since 2001, he has been with the China University of Mining and Technology, where he is currently the Deputy Director of Jiangsu Province Laboratory of Electric and Automation. He has been awarded 14 patents and published two books and over 50 conference and journal publications. His current research interests include the protection in power grid, critical electrical equipment assessment, and modeling in energy interconnection.

TIANYU HOU received the B.S. degree in electrical engineering from Shandong University, Jinan, China, in 2018. He is currently pursuing the M.S. degree in electrical engineering with the China University of Mining and Technology, Xuzhou, China. His main research interests include traveling wave fault location and power system protection.

GUANHUA WANG received the B.S. degree in electrical engineering from the Chongqing University of Technology, Chongqing, China, in 2018. He is currently pursuing the M.S. degree in electrical engineering with the China University of Mining and Technology, Xuzhou, China. His main research interests include traveling wave fault location and power system protection.

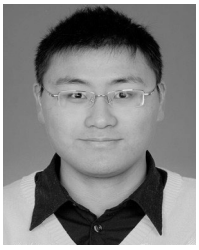

XUAN CHEN received the B.S. degree in electrical engineering from Southeast University, Nanjing, China, in 2011. He is currently a Scientific and Technological Information Manager with State Grid Jiangsu Electric Power Company Maintenance Branch. His main research interest includes power system.

SONG TENG received the B.S. degree in electrical engineering from the Anhui University of Technology, Ma'anshan, China, in 2010, and the M.S. degree in electrical engineering from North China Electric Power University, Beijing, China, in 2013. He is currently a Scientific and Technological Information Manager with State Grid Xuzhou Electric Power Company. His main research interest includes flexible high-voltage direct current (HVDC) transmission technology.